Journal of Sound and Vibration 327 (2009) 26–40

Contents lists available at ScienceDirect

Journal of Sound and Vibration

journal homepage: www.elsevier.com/locate/jsvi

Frequency analysis of a heterogeneous perforated panel using a super-element formulation

Y. Yang, A.S. Fallah *, L.A. Louca

Department of Civil and Environmental Engineering, Imperial College London, South Kensington Campus SW7 2AZ, UK

ARTICLE INFO

Article history:
Received 3 December 2008
Received in revised form
12 March 2009
Accepted 12 May 2009
Handling Editor: C.L. Morfey
Available online 12 June 2009

ABSTRACT

Heterogeneous perforated panels represent a wide class of structural elements with holes where perforations and matrix are of dissimilar materials e.g. metallic member of a perforated hybrid joint with resin-fillings. There is a variety of objectives for introducing holes e.g. weight saving or mechanical interlock. Where there is a regular pattern to the arrangement of holes the perforated element can be assimilated to a lattice. In the present study, numerical analysis has been conducted on investigating the shock frequency filtering phenomenon encountered in two-dimensional (2D) lattice structures. A super-element of the primitive cell (unit cell) of the lattice has been formulated and applied in conjunction with the Floquet–Bloch's principle to study the shock response characteristics. Plane wave propagation is investigated by constructing the first Brillouin zone of the primitive cell in associated Fourier space (*k*-space). The frequency characteristics are presented in the band structure diagram. The study emphasizes the existence of frequency pass and stop bands and the extent of this phenomenon. The frequency filtering effects of the heterogeneous perforated 2D lattice has shown its potential value to improve the structural performance of perforated hybrid joints subjected to dynamic loads.

1. Introduction

A lattice has been defined in mathematical abstraction as a regular periodic arrangement of points in space [1]. This arrangement is also referred to as lattice points which along with the basis vectors form the reticulated periodic/lattice structure. Ideal periodic structures are specified as structures constructed by regular repetition in space of identical primitive/unit cell along predefined directions [2,3].

Many researches have carried out studies of wave propagation in such structures. Brillouin conducted a comprehensive review of the early works on wave propagation in periodic structures as early as 1953 with the history of the subject being traced back to early 1680s, which included contributions by Newton, Taylor, Bernoulli, Clairaut, Euler, Lagrange, and Baden-Powell. However, till the end of the 18th century, the main analytical model of systems considered comprised lumped masses joined by massless springs [4]. This model was sufficient to enable a study of the idea of free wave propagation in such structures to be conducted. Rayleigh solved the governing wave equation for a stretched string with a periodic and continuous variation of density along its length using Hill's method [5]. The lattice structure was initially investigated with atomic models of crystals in the field of solid state physics in the early 20th century following the discovery of X-ray diffraction and the publication of simple and reasonably successful prediction of crystalline properties [6]. From the early

* Corresponding author. Tel: +44 0 20 75946028; fax: +44 0 20 72252716.
E-mail address: as3@imperial.ac.uk (A.S. Fallah).

0022-460X/$ - see front matter © 2009 Elsevier Ltd. All rights reserved.
doi:10.1016/j.jsv.2009.05.017

research on crystal diffraction, it was found that although the reflection from each plane of the lattice points is assumed to be specular, only for certain values of the angle of entering beam light θ will the reflections from all parallel planes add up in phase to give a strong diffracted beam [7]. This is the well-known Bragg's law: $2d\sin\theta = n\lambda$, which is a consequence of the periodicity of the space lattice. Based on this, Floquet–Bloch's principle [8] and band theory of solids were derived [9]. First Brillouin zone was also introduced, which is the smallest volume entirely enclosed by planes that are the perpendicular bisectors of the reciprocal lattice vectors drawn from the origin. Any vector $\mathbf{k}$ from the origin to the boundary of the Brillouin zone will satisfy the Bragg equation (i.e. the diffraction condition). The methodology of using Floquet–Bloch's principle and band theory to analyse the frequency character of a lattice structure has been applied for studying both electromagnetic waves in a crystal [10,11] and light or sound waves in a periodic structure [12–14]. There has been a growing interest in wave propagation through man-made structures. Researchers are showing the band structure can be designed in an artificial fashion to suit different design requirement [15]. Applications are mainly developed in the fields of electricity, optics and quantum physics. For instance, particular photonic band structure can now be designed in photonic-bandgap materials (PBG), which means a transparent material can become opaque for any light wave vector [16]. One of the advantages of PBG materials is that the underlying theory can also be applied to other types of waves like electromagnetic or sound waves. The theory has been widely extended and employed in various branches of science: in electronics to design an insulator or a conductor [17,18]. Analogously, in acoustics, noise control devices have been developed [19,20] and designable acoustic band gaps for two-dimensional (2D sonic crystals were presented by Lai [21]. These works have led to a renewed interest in elastic wave propagation in lattice structures in structural and mechanical field [22].

Recently, literature shows that the frequency filtering phenomena for lattice structures can be exploited in structural and mechanical design. Researchers have proved the advantages of applying a lattice structure in sandwich beams, panels [23–26] and in truss structures [27]. From these studies it can be seen, in general, that wave propagation in periodic lattices is fundamentally different from that occurring in a homogeneous medium.

The concept of applying perforations to the metal part of hybrid joints was first addressed by Unden [28]. The original purpose of the introduction of perforations is to increase the cohesion between plain metal plates and adjacent layers of fibre-reinforced plastic matrix, hence to improve the transfer of load into fibre-reinforced plastic part. Apart from the benefit of mechanical interlocking, the perforated steel plate is also believed to decrease the elastic mismatch between the stiff steel and the relatively compliant fibre reinforced composite. This design was further investigated and improved by Grenestedt et al. [29,30]. Their research suggested that under static tensile load circumstances, shape of the perforation did not affect the strength of the hybrid joint. Their experimental data revealed that the joint with perforations had highest strength when it comprised 7–9 rows of holes. This nominally optimally perforated strips yielded 25–30% higher than their non-perforated counterparts. However, most of the recent works are focused on perforated joints under static loads. The perforated joint was primarily used to improve the mechanical interlock, and reduce the stress concentration owing to stiffness mismatch.

In this paper, the dynamic shock response of a heterogeneous perforated 2D lattice is investigated with high interest in the frequency filtering effects. Although this study is carried out for a generic condition, if we consider the heterogeneous perforated 2D lattice as the representative of a typical metal-composite hybrid joint shown in Fig. 1 with perforations on the metal part, and the holes are filled in with resin material, then, the perforation does not only benefit the joint by tackling the elastic mismatch and sudden load transfer issues, but also brings the anticipated advantage of frequency filtering features to the joint. Hence, it can potentially improve the overall performance of the joint under dynamic loads. The main methodologies applied in this research are explained as following.

By applying the isoparametric finite element formulation [31], a super-element is formulated for the primitive cell instead of using the global assumed modes method to solve the governing differential equations i.e. Navier or Beltrami–Michell equations, since it is extremely difficult if not impossible to choose a set of global shape functions, ψ_i for a structure with complex geometry [32]. The formulation is explained in Section 2 of the present work.

A plane wave solution is admitted for the conducted frequency analyses. Thus, the generalised coordinate of a lattice point of a harmonically vibrating infinite system is equal to $e^{\pm\mathbf{k}}$ multiplied by that of its neighbour with the plus/minus sign being contingent upon the direction of the wave motion. $\mathbf{k}$ is a complex vector in general the components of which have real and an imaginary parts, say $k_j = \delta_j + \mathrm{i}\varepsilon_j$, where the real part δ_j is the attenuation constant and the imaginary part

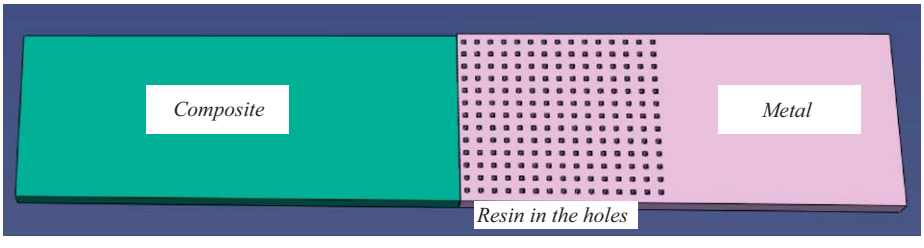

Fig. 1. Typical perforated hybrid joint.

ε_j is the phase constant. For waves propagating without attenuation, the real part is zero. Floquet–Bloch's principle is applied in the present study.

It states that the eigenfunctions of the wave equation for a periodic potential are of the form of the product of a plane wave $e^{i\mathbf{k}\cdot\mathbf{r}}$ and a function $u_{\mathbf{k}}(\mathbf{r})$ with the periodicity of the lattice: $\psi_{\mathbf{k}}(\mathbf{r}) = \mathbf{u}_{\mathbf{k}}(\mathbf{r})\, e^{i\mathbf{k}\cdot\mathbf{r}}$, where $\mathbf{r}$ denotes the lattice points in a unit cell. The subscript $\mathbf{k}$ indicates that the function $u_{\mathbf{k}}(\mathbf{r})$ depends on the wave vector $\mathbf{k}$, and $u_{\mathbf{k}}(\mathbf{r})$ denote the displacement of a lattice point in the reference unit cell, which has the period of the lattice with $u_{\mathbf{k}}(\mathbf{r}) = u_{\mathbf{k}}(\mathbf{r} + \mathbf{T}_{\mathbf{L}})$, here $\mathbf{T}_{\mathbf{L}}$ is a translation vector of the lattice. Therefore, in our case, the global shock response of the infinitely periodic 2D lattice under plane wave propagation can be studied by analysing the smallest repetitive unit, i.e. the primitive cell. Sigmund et al. [33] and Fleck et al. [34] have applied similar methods to study the plane wave propagation in 2D lattices. The former study uses a systematic approach based on topology optimisation procedures to study a square arrangement of inclusions, and by varying the proportion of inclusion to the matrix; they found that the maximum width of band gap appears for the high contrast case. The latter explored wave propagation phenomena in three regular honey combs, and concluded that the slenderness ratio of the constituent beams of the lattice has a significant influence on the band structure. This analytical method is used in this paper to obtain the frequency characters of the heterogeneous perforated 2D lattice.

Based on the foregoing discussion, the objectives of the current paper are: to define and formulate a super-element of the primitive cell by programming a displacement based FE code in MATLAB, to apply the static condensation technique in order to decrease the size of the stiffness and mass matrices and finally, in conjunction with the super-element formulation, to perform a frequency analysis of the primitive cell using Floquet–Bloch's principle. The position of the unit cell is immaterial as long as an infinite lattice is concerned and shock attenuation is negligible. Wave propagation frequencies are calculated from the deduced complex eigenvalue problem and wave dispersion surfaces are obtained in wave vector space (k-space). From the deduced band structure diagrams, the shock response of a sample heterogeneous perforated 2D lattice is explored.

This work is organised into five sections: After the introduction, the finite element formulation is explained in Section 2. This is followed by the super-element formulation of the primitive cell by MATLAB programming as elucidated in Section 3. By using the super-element formulation, the frequency analysis was conducted and the results are presented in Section 4. Finally, the results are concluded and a brief discussion is followed.

2. Finite element formulation

2.1. Primitive cell

A primitive cell was selected to investigate the structural behaviour of the perforated panel shown in Fig. 2a. Considering all axes of symmetry, the primitive cell is divided into four quarters, as shown in Fig. 2b. The geometric configuration of the primitive cell is governed by parameters a, b, and c as defined by Fig. 2b. Since the lattic studied here is in 2D space (say in x–y plane), the thickness of the perforated panel t is set to unity. The material input properties of the steel panel and resin inclusions are tabulated in Table 1.

2.2. Lagrangian FE formulation

As shown in Fig. 2b, each quarter of the primitive cell is discretized into four Lagrangian elements labelled I–IV. The shape function orders of the elements in the lattice panel can then be controlled by using input parameters N, M and P as

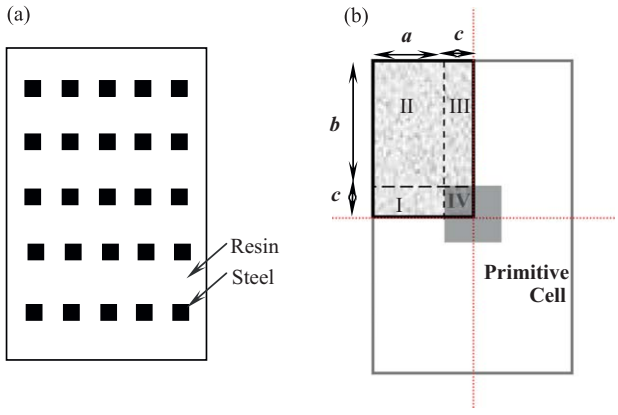

Fig. 2. (a) A perforated panel with square hold lattices, (b) a primitive cell with parametric geometric input: a, b, c ($c<a<b$).

Table 1
2D Panel material properties.

Steel: Young's modulus $E_s = 195$	**Resin**: Young's modulus $E_r = 3$
Poisson's ratio $\upsilon_s = 0.3$	Poisson's ratio $v_r = 0.25$
Mass density $\bar{\rho}_s = 8.06\text{E}-6$	Mass density $\bar{\rho}_r = 1.7\text{E}-6$

Units: mm, ms, kg, kN, GPa.

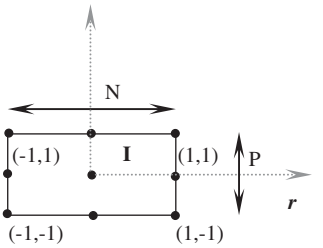

Fig. 3. Lagrangian element. Here using 3×3 Lagrangian element as an example (i.e. $N = 3$, $P = 3$).

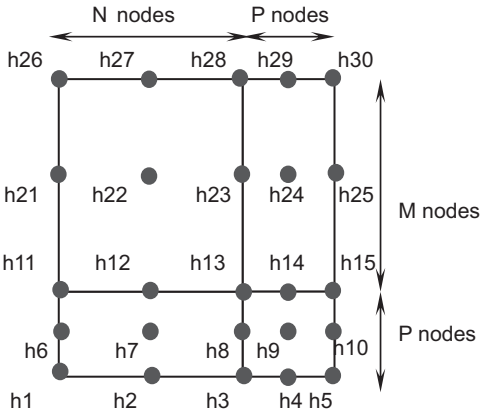

Fig. 4. Quarter of the primitive cell assembled by four 3×3 Lagrangian elements.

numbers of nodes on each edge of the Lagrangian element. As an example, a 3×3 Lagrangian element I is shown in Fig. 3 with $N = 3$ and $P = 3$. Parameters r and s specify the natural coordinates and vary between -1 and 1 (Fig. 4).

As we are considering the shock response in a 2D lattice, the Lagrangian element is assumed to have two degrees of freedom at each point $\mathbf{U} = (U,V)$ corresponding to coordinates in the (x, y) plane. The displacement field within the element $\mathbf{u}$ for a typical Lagrangian element (Fig. 3) is thus related to the nodal displacement vector $\mathbf{U}$ as follows:

$$\mathbf{u}^{(\mathbf{LI})}(x,y) = \mathbf{H}^{(\mathbf{LI})}(x,y)\mathbf{U} \tag{1}$$

where $\mathbf{H}^{(\mathbf{LI})}$ is the displacement interpolation matrix, the superscript (LI) denotes Lagrangian element I. Here, we applied MATLAB scripts 1 and 2 (shown in Appendix B) to deduce the shape functions of the Lagrangian element I in symbolic form. An example shape function matrix $\mathbf{HI}^{\mathbf{T}}$ of a 3×3 Lagrangian element is shown in Appendix A. The Jacobian operator can be derived from Eq. (2). The Jacobian operator derived for a 3×3 Lagrangian element was recorded in Appendix B as an instance.

$$\mathbf{J} = \begin{bmatrix} \dfrac{\partial \mathbf{U}}{\partial r} & \dfrac{\partial \mathbf{V}}{\partial r} \\ \dfrac{\partial \mathbf{U}}{\partial s} & \dfrac{\partial \mathbf{V}}{\partial s} \end{bmatrix} \tag{2}$$

By using Gauss integration, element mass and stiffness matrices, $\mathbf{M_e}$ and $\mathbf{K_e}$ are calculated in Eqs. (3) and (4), respectively. The related MATLAB script 4 is given in Appendix C.

$$\mathbf{M_e} = \int_{\mathbf{v}} \rho \mathbf{H}^{\mathbf{T}}\mathbf{H}\,\mathbf{dV} = \rho \mathbf{t} \cdot \int_{-1}^{1}\int_{-1}^{1} \mathbf{\Gamma}\,dr\,ds \tag{3}$$

where $\mathbf{\Gamma} = \mathbf{H}^{\mathbf{T}} \cdot \mathbf{H} \cdot \det \mathbf{J}$.

The mass matrix of Part I of the primitive cell, $\mathbf{M_{el}}$, which derived for a 3×3 Lagrangian element, is given in Appendix D. It indicates there is a linear relationship between the mass matrix and geometric inputs a and c. Similarly, it can be shown that the mass matrix for Part II is also linearly dependent upon a and b.

The stress–strain constitutive matrix, $\mathbf{C}$ (shown in Eq. (5)) corresponding to plane stress condition is used in the present study:

$$\mathbf{K_e} = \int_{\mathbf{V}} \mathbf{B^T C B}\, \mathbf{dV} = t \cdot \int_{-1}^{1}\int_{-1}^{1} \mathbf{\Lambda}\, \mathrm{d}r\, \mathrm{d}s \tag{4}$$

$$\mathbf{C} = \frac{E}{1-\nu^2}\begin{bmatrix} 1 & \nu & 0 \\ \nu & 1 & 0 \\ 0 & 0 & \dfrac{1-\nu}{2} \end{bmatrix} \tag{5}$$

$$\mathit{\Lambda} = \mathbf{B^T C B} \cdot \det \mathbf{J} \tag{6}$$

where $\mathbf{B}$ is the strain–displacement matrix. E is the Young's Modulus; υ is the Poisson's ratio. The stiffness matrix of Part I of the primitive cell, $\mathbf{K_e}$ derived from a 3×3 Lagrangian element is given in Appendix D. It indicates that there is a functional dependence of k_{ij} on ζ ($\zeta = c/a$).

2.3. Assembly

By applying the standard direct stiffness method, both mass and stiffness matrices ($\mathbf{M_e}$ and $\mathbf{K_e}$) of the four Lagrangian elements, I, II, III and IV, can be assembled into the system displacement coordinates. Hence, it forms a quarter of the primitive cell with mass matrix $\mathbf{M_{TL}}$ and stiffness matrix $\mathbf{K_{TL}}$, which renders the primitive cell element formulation possible.

3. Super-element formulation

3.1. Transformation matrices

After assembling, both mass and stiffness of the top left (TL) quarter of the primitive cell is derived (shown in Fig. 2b). By using the symmetric character of the primitive cell, transformation matrices $\mathbf{A}$ given in Eq. (7) can be applied in Eq. (8) to form the mass and stiffness matrices of the other three quarters of the primitive cell. Here we take $\mathbf{A_{TR}}$ as an example, the non-zero entries of the matrix is formed by repeating a blog of 2×2 entries $[-1, 0; 0, 1]$ along the diagonal. The repeating time is equal to half of the degree of freedom (dof) of each quarter of the unit cell. So the size of the transformation matrices is always equal to the size of the mass or stiffness matrix, which is governed by the input parameters of the Lagrangian elements: N, M and P.

$$\mathbf{A_{TR}} = \begin{bmatrix} -1 & 0 & & & \\ 0 & 1 & & & \\ & & \ddots & & \\ & & & -1 & 0 \\ & & & 0 & 1 \end{bmatrix}_{\mathrm{DOF}/2} \quad \mathbf{A_{BL}} = \begin{bmatrix} 1 & 0 & & & \\ 0 & -1 & & & \\ & & \ddots & & \\ & & & 1 & 0 \\ & & & 0 & -1 \end{bmatrix}_{\mathrm{DOF}/2} \quad \mathbf{A_{BR}} = \begin{bmatrix} -1 & 0 & & & \\ 0 & -1 & & & \\ & & \ddots & & \\ & & & -1 & 0 \\ & & & 0 & -1 \end{bmatrix}_{\mathrm{DOF}/2} \tag{7}$$

where the subscripts (TR), (BL), and (BR) denote the top right, bottom left, and bottom right quarter of the primitive cell, respectively.

$$\hat{\mathbf{K}} = \mathit{Renumber}\langle \hat{\mathbf{A}}\mathbf{K_{TL}}\hat{\mathbf{A}}^{\mathbf{T}} \rangle \quad \hat{\mathbf{M}} = \mathit{Renumber}\langle \hat{\mathbf{A}}\mathbf{M_{TL}}\hat{\mathbf{A}}^{\mathbf{T}} \rangle \tag{8}$$

Here the head is applied to denote the corresponding subscripts. For instance, $\mathbf{K_{TR}} = \mathit{Renumber}\langle \mathbf{A_{TR}}\mathbf{K_{TL}}\mathbf{A_{TR}^T} \rangle$. As the transformation matrices mirror the mass and stiffness matrices, entries in each matrix are in the reverse order, which needs to be renumbered.

3.2. Modal parametric mass and stiffness matrices

By using the same approach (i.e. the direct stiffness method), the four quarters of the primitive cell are assembled together, hence, it forms the super-element matrix with the stiffness matrix $\mathbf{K_C}$, and mass matrix $\mathbf{M_C}$.

$$\mathbf{K_C} = \sum \hat{\mathbf{K}} = \mathbf{K_{TL}} + \mathbf{K_{TR}} + \mathbf{K_{BL}} + \mathbf{K_{BR}} \tag{9}$$

$$\mathbf{M_C} = \sum \hat{\mathbf{M}} = \mathbf{M_{TL}} + \mathbf{M_{TR}} + \mathbf{M_{BL}} + \mathbf{M_{BR}} \tag{10}$$

To validate the accuracy, several element tests have been conducted. By comparing the displacement output from a commercial software package (ABAQUS 6.7-1) FE model and the super-element formulation under both static and dynamic edge loading conditions, it is seen that even by using a super-element with 50 degrees of freedom, which is composed of sixteen 2×2 Lagrangain elements, good correlation can be obtained compared to the ABAQUS model with CPS8, 8-node biquadratic elements. The error is less than 0.2% under static load and less than 5% error under dynamic load for frequencies below twice the tensile mode frequency. The mass and stiffness matrices of the super-element also show there is a direct relationship between the geometric ratios $\zeta = c/a$ and $\eta = c/b$ and $\mathbf{K_C}$ and $\mathbf{M_C}$, which indicates shock response characteristics of a heterogeneous perforated panel can be controlled by ζ and η, and as we expected, some frequency filtering could be achieved. This will be discussed in next section.

4. Frequency analysis

Based on the formulated super-element, a frequency analysis of the heterogeneous perforated 2D lattice was conducted. According to Bloch's theorem, the displacement at the jth point in any cell can be expressed as:

$$u(\mathbf{r}) = u(\mathbf{r}_j)\, e^{\mathbf{k}\cdot(\mathbf{r}-\mathbf{r}_j)} = u(\mathbf{r}_j)\, e^{(\mathbf{k}_1\cdot\mathbf{n}_1+\mathbf{k}_2\cdot\mathbf{n}_2)} \tag{11}$$

where $u(\mathbf{r}_j)$ is the displacement of a lattice point in the primitive cell; the integer pair $(\mathbf{n}_1,\mathbf{n}_2)$ is used to identify translations along the $\mathbf{e_1}$ and $\mathbf{e_2}$ direction, respectively; vector $\mathbf{r}$ is defined as: $\mathbf{r} = \mathbf{r_j}+\mathbf{n_1e_1}+\mathbf{n_2e_2}$; and $k_1 = \delta_1+i\varepsilon_1$ and $k_2 = \delta_2+i\varepsilon_2$ represent the components of the wave vector $\mathbf{k}$ along $\mathbf{e_1}$ and $\mathbf{e_2}$. i.e. $k_1 = \mathbf{k}\cdot\mathbf{e_1}$, and $k_2 = \mathbf{k}\cdot\mathbf{e_2}$. Assumption has been made that there is no attenuation for the wave propagation studied in this paper. Hence, the variation of complex wave amplitude across a primitive cell does not depend upon the location of the primitive cell within the structure. Thus, the shock response of the 2D lattice can be investigated by considering wave motion within a single primitive cell shown in Fig. 5. For computational convenience purposes, the 2D lattice panel is transformed from real space domain to the reciprocal lattice in the k-space where solution of the problem is simpler.

The basis vectors of the two systems are related by:

$$\mathbf{e}_i \cdot \mathbf{e}_j^* = 2\pi \cdot \delta_{ij}$$

$$\mathbf{e}_1 = 2(a+c)\,\vec{\mathbf{i}}; \quad \mathbf{e}_2 = 2(b+c)\,\vec{\mathbf{j}}$$

$$\mathbf{e}_1^* = \frac{2\pi}{2(a+c)}\,\vec{\mathbf{j}}; \quad \mathbf{e}_2^* = \frac{2\pi}{2(b+c)}\,\vec{\mathbf{i}} \tag{12}$$

where $\mathbf{e}_i$ denotes the basis vectors of the direct lattice and $\mathbf{e}_j^*$ denotes the basis of reciprocal lattice and δ_{ij} is the Kronecker delta function. For a 2D lattice, the subscripts $i, j \in \{1,2\}$. The headed $\vec{\mathbf{i}}$ and $\vec{\mathbf{j}}$ are the unit vectors.

4.1. Static condensation

For computational efficiency, the super-element is modified by static condensation, which condensed the internal degrees of freedom; hence the total dof of the primitive cell reduces from 50 to 32. A brief process of the static condensation is introduced here:

$$\begin{bmatrix} \mathbf{M_{aa}} & \mathbf{0_{ad}} \\ \mathbf{0_{da}} & \mathbf{0_{dd}} \end{bmatrix} \begin{Bmatrix} \ddot{\mathbf{U}}_\mathbf{a} \\ \ddot{\mathbf{U}}_\mathbf{d} \end{Bmatrix} + \begin{bmatrix} \mathbf{K_{aa}} & \mathbf{K_{ad}} \\ \mathbf{K_{da}} & \mathbf{K_{dd}} \end{bmatrix} \begin{Bmatrix} \mathbf{U_a} \\ \mathbf{U_d} \end{Bmatrix} = \begin{Bmatrix} \mathbf{P_a(t)} \\ \mathbf{0_d} \end{Bmatrix} \tag{13}$$

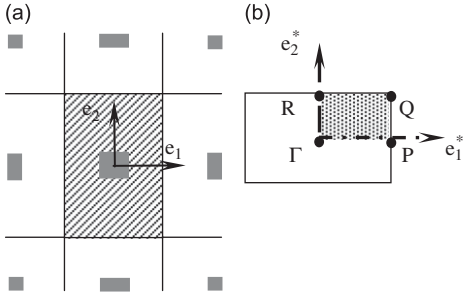

Fig. 5. A heterogeneous perforated 2D lattice: (a) with a selected primitive cell and the first Brillouin zone and (b) in k space. The irreducible part of the first Brillouin zone are shown as shaded area. The basis vectors of the direct lattice (e_i) and the reciprocal lattice e_i^* are also shown. The points are defined in Table 2.

Table 2
The irreducible first Brillouin zone points.

Γ	P	Q	R
0, 0	$\frac{\pi}{2(a+c)}, 0$	$\frac{\pi}{2(a+c)}, \frac{\pi}{2(b+c)}$	$0, \frac{\pi}{2(b+c)}$

The wave vectors are chosen along the locus ΓPQR in reciprocal lattice.

where the subscript a denotes the active degrees of freedom, in this case they are the entries on the boundary of the primitive cell, and d corresponds to condensed ones, which are the internal ones.

Given the equation of motion in partitioned-matrix form which provides a static constraint equation:

$$\mathbf{K_{da}U_a} + \mathbf{K_{dd}U_d} = \mathbf{0_d} \tag{14}$$

Then the static condensation transformation matrix is

$$\mathbf{T_c} \equiv \begin{bmatrix} \mathbf{I_{aa}} \\ \mathbf{T_{da}} \end{bmatrix} = \begin{bmatrix} \mathbf{I_{aa}} \\ -\mathbf{K_{dd}^{-1}K_{da}} \end{bmatrix} \tag{15}$$

And the condensed mass and stiffness matrices can be derived by:

$$\mathbf{M_{aa}} = \mathbf{T_c^T M_c T_c} \quad \text{and} \quad \mathbf{K_{aa}} = \mathbf{T_c^T K_c T_c} \tag{16}$$

where $\mathbf{M_c}$ and $\mathbf{K_c}$ are the uncondensed mass and stiffness matrix of the primitive cell obtained from Eqs. (9) and (10). $\mathbf{M_{aa}}$ and $\mathbf{K_{aa}}$, are the condensed mass and stiffness matrix of the primitive cell.

The first Brillouin zone is defined as a Wigner–Seitz or primitive unit cell of the reciprocal lattice, and it can be formed by constructing the perpendicular bisectors of the edges of the reciprocal primitive cell. Thus, the wave vectors can be restricted to the edges of the irreducible part of the first Brillouin zone in the reciprocal lattice presented in Fig. 5b by the shaded region, and the lattice points of the irreducible first Brillouin zone in associated Fourier space are tabulated in Table 2. This allows the bandgaps character of the heterogeneous perforated 2D lattice to be investigated, since the band extrema occurs along the boundaries of the irreducible zone.

The geometric inputs a, b, and c are converted into dimensionless parameters using Buckingham's Pi-theorem as follows:

$$\alpha = C/A, \quad \beta = C/B; \tag{17}$$

where the width of the unit cell $A = 2(a+c)$, the length of the unit cell $B = 2(b+c)$ and the width of the square resin hole $C = 2c$.

The following two cases have been investigated in the frequency analysis:

$$\alpha = \frac{1}{12}, \quad \beta = \frac{1}{24};$$

$$\alpha = \frac{1}{3}, \quad \beta = \frac{1}{6}. \tag{18}$$

4.2. Floquet–Bloch's principle

In solid state physics, band-structure theory has been successfully applied to analyse the diffraction of the waves by crystals to determine the ground-state properties such as cohesive energies or crystallographic structure [35]. In contrast, Bloch's theorem is used here to predict and estimate the shock response of a 2D lattice under plane wave by investigating one primitive cell with a given configuration. By applying Bloch's theorem, which can be rewritten as $u_{\mathbf{nk}}(\mathbf{r}_j + \mathbf{T_L}) = u_{\mathbf{nk}}(\mathbf{r}_j)\, e^{\mathbf{ik}\cdot\mathbf{r}_j}$ where n is the band index, and $\mathbf{T_L}$ is a translation vector of the lattice, the following relations between the displacements can be obtained:

$$\mathbf{u}_5 = \mathbf{u}_1 e^{\mathbf{k}_1}, \quad \mathbf{u}_9 = \mathbf{u}_6 e^{\mathbf{k}_1}, \quad \mathbf{u}_{10} = \mathbf{u}_7 e^{\mathbf{k}_1}, \quad \mathbf{u}_{11} = \mathbf{u}_8 e^{\mathbf{k}_1},$$

$$\mathbf{u}_{12} = \mathbf{u}_1 e^{\mathbf{k}_2}, \quad \mathbf{u}_{13} = \mathbf{u}_2 e^{\mathbf{k}_2}, \quad \mathbf{u}_{14} = \mathbf{u}_3 e^{\mathbf{k}_2}, \quad \mathbf{u}_{15} = \mathbf{u}_4 e^{\mathbf{k}_2}, \quad \mathbf{u}_{16} = \mathbf{u}_1 e^{\mathbf{k}_1 + \mathbf{k}_2} \tag{19}$$

where the subscripts, respectively, specify the displacements nodes of a condensed super-element, as shown in Fig. 6. The above relationships can be defined in the matrix notation as:

$$\mathbf{u} = \mathbf{T_B}\tilde{\mathbf{u}} \tag{20}$$

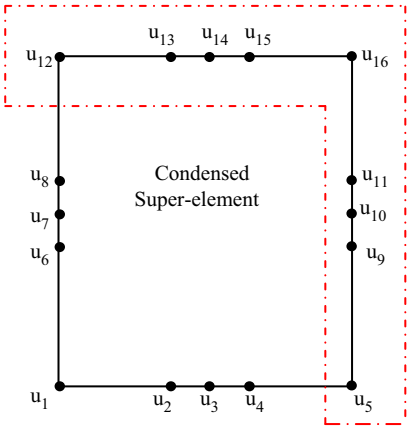

Fig. 6. A condensed super-element (the nodes outside the red block show the Bloch reduced coordinates). (For interpretation of the references to color in this figure legend the reader is referred to the web version of this article.)

$$\mathbf{T_B} = \begin{bmatrix} \mathbf{I} & 0 & 0 & 0 & 0 & 0 & 0 \\ 0 & \mathbf{I} & 0 & 0 & 0 & 0 & 0 \\ 0 & 0 & \mathbf{I} & 0 & 0 & 0 & 0 \\ 0 & 0 & 0 & \mathbf{I} & 0 & 0 & 0 \\ \mathbf{I}e^{\mathbf{k}_1} & 0 & 0 & 0 & 0 & 0 & 0 \\ 0 & 0 & 0 & 0 & \mathbf{I} & 0 & 0 \\ 0 & 0 & 0 & 0 & 0 & \mathbf{I} & 0 \\ 0 & 0 & 0 & 0 & 0 & 0 & \mathbf{I} \\ 0 & 0 & 0 & 0 & \mathbf{I}e^{\mathbf{k}_1} & 0 & 0 \\ 0 & 0 & 0 & 0 & 0 & \mathbf{I}e^{\mathbf{k}_1} & 0 \\ 0 & 0 & 0 & 0 & 0 & 0 & \mathbf{I}e^{\mathbf{k}_1} \\ \mathbf{I}e^{\mathbf{k}_2} & 0 & 0 & 0 & 0 & 0 & 0 \\ 0 & \mathbf{I}e^{\mathbf{k}_2} & 0 & 0 & 0 & 0 & 0 \\ 0 & 0 & \mathbf{I}e^{\mathbf{k}_2} & 0 & 0 & 0 & 0 \\ 0 & 0 & 0 & \mathbf{I}e^{\mathbf{k}_2} & 0 & 0 & 0 \\ \mathbf{I}e^{(\mathbf{k}_1+\mathbf{k}_2)} & 0 & 0 & 0 & 0 & 0 & 0 \end{bmatrix} \quad \tilde{\mathbf{u}} = \begin{bmatrix} \mathbf{u}_1 \\ \mathbf{u}_2 \\ \mathbf{u}_3 \\ \mathbf{u}_4 \\ \mathbf{u}_6 \\ \mathbf{u}_8 \\ \mathbf{u}_{10} \end{bmatrix}$$

where $\tilde{\mathbf{u}}$ is the displacements of the nodes in the Bloch reduced coordinates, and $\mathbf{I}$ is the 2nd order identity matrix.

4.3. Analysis of free wave motion

For a free vibration, the governing differential equation of the finite element model of the primitive cell takes the form:

$$\mathbf{M}\ddot{\mathbf{u}} + \mathbf{K}\mathbf{u} = 0 \tag{21}$$

By applying Bloch's theorem it follows that:

$$\tilde{\mathbf{D}}\tilde{\mathbf{u}} = 0, \text{ where } \tilde{\mathbf{D}} = \mathbf{T}_\mathbf{B}^\mathbf{H}\mathbf{D}\mathbf{T}_\mathbf{B}, \tag{22}$$

The dynamic stiffness $\mathbf{D}$ is defined as: $\mathbf{D} = [\mathbf{K} - \Omega\mathbf{M}]$, and $\Omega = \omega^2$; the superscript H denotes the Hermitian transpose. Therefore, a linear algebraic eigenvalue problem is formulated as follows:

$$\tilde{\mathbf{D}}(\mathbf{k}_1, \mathbf{k}_2, \Omega)\tilde{\mathbf{u}} = 0 \tag{23}$$

As the assumption of no attenuation has been taken into this 2D shock wave analysis, (i.e. $k_1 = \mathrm{i}\varepsilon_1$ and $k_2 = \mathrm{i}\varepsilon_2$), the associated eigenvalue problem only includes two components of the wave vector viz. the phase constants ε_1 and ε_2 along with the frequency of the plane wave ω.

As discussed earlier, due to the periodicity, the phase constants ε_1 and ε_2 can be specified to restrict the wave vector to the edges of the irreducible part of the 1st Brillouin zone (i.e. $\mathbf{k} \in [-\pi, \pi]^d$, where d is the dimension). Any other point $\mathbf{k}$ of the zone which is not in this rectangle can be rotated into a $\mathbf{k}$-vector inside the rectangle by a symmetry operation that

leaves the zone invariant. Based on these, dispersion surfaces can be computed by solving for the frequencies. The results are presented and discussed in the next section.

4.4. Band structure

If we take the square hole size, $c = 2$ mm and $c = 0.5$ mm for Cases 1 and 2, respectively, from [24] it gives:

- Case1: $a = 4$ mm, $b = 10$ mm;
- Case 2: $a = 5.5$ mm, $b = 11.5$ mm

and the corresponding irreducible first Brillouin zone points are shown in Table 3.

By solving the resulting linear algebraic eigenvalue problem in Eq. (29), eigenvalues Ω for each pair of wave vector components k_1 and k_2 are calculated. Also, the obtained frequencies are normalised by dividing the first none zero frequency at Γ.

$$\text{i.e. } \hat{\omega}_i = \omega_i/\omega_{\Gamma 3} \tag{24}$$

The dispersion surfaces for the seven lowest frequencies are attained and plotted in Figs. 7 and 8. The parameter s is introduced as a scalar pathlength parameter in k space, along the perimeter $\Gamma PQR\Gamma$ of the shaded region ΓPQR i.e. the first Brillouin zone. It is used to indicate the location of any point on the perimeter. The horizontal axes denote values of s, the k-space position on the boundary of the irreducible Brillouin zone. Firstly, from both cases, as expected, it can be seen that there is a range of frequencies with no corresponding eigenmodes, i.e. there is a completed forbidden band between the fourth and fifth bands in both cases. This means within the forbidden band, there is no elastic wave with the frequencies of the band that can propagate through the structure. The forbidden band zone is indicated with shaped regions in Figs. 7 and 8.

Secondly, it can also be noticed that by increasing the ratios α and β, apart from the forbidden band between the fourth and fifth bands, there is an additional complete band-gap between sixth and seventh band shown in Fig. 8. This means that,

Table 3
The irreducible first Brillouin zone points for $c = 2$, $\alpha = 0.5$, $\beta = 0.2$; and $c = 0.5$.

Γ	P	Q	R
0, 0	$\frac{\pi}{12}, 0$	$\frac{\pi}{12}, \frac{\pi}{24}$	$0, \frac{\pi}{24}$

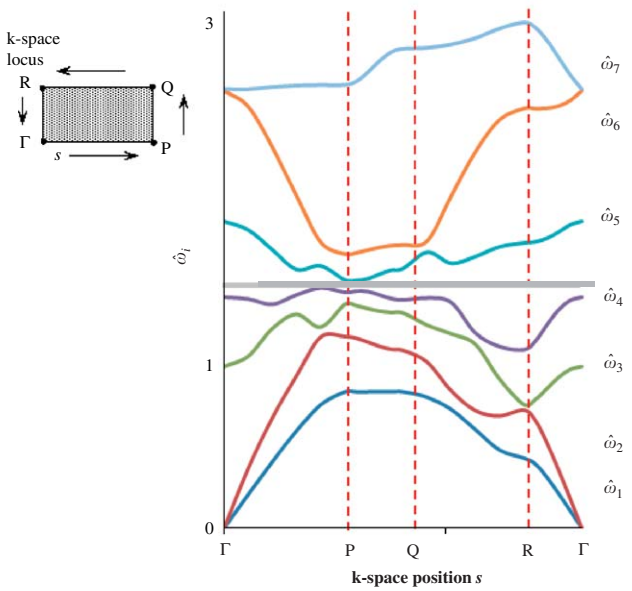

Fig. 7. Band structure diagram for Case 1.

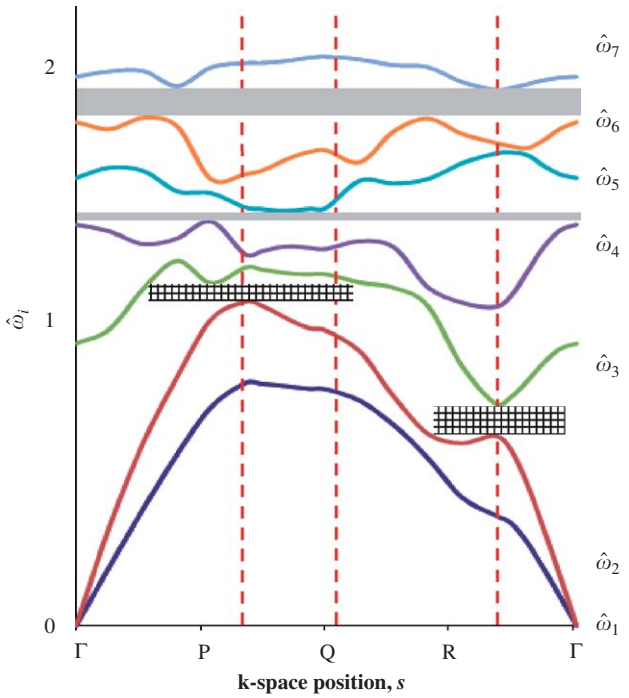

Fig. 8. Band structure diagram for Case 2.

as expected, the 2D lattice does have the frequency filtering effects. Furthermore, by varying the geometric input ratios α and β, the band structure diagram can be designed. Thus, a desired shock response of a hybrid joint can be achieved by choosing the suitable perforation.

Last but not least, Figs. 7 and 8 also indicate that perforations will have limited effects to lower excitation frequencies. As it shows in Fig. 8, there is no full stop band in the lower frequencies domain. Nevertheless, the two partial band gaps, which are indicated with hatched regions in the diagram, shows there will still be propagation at those frequencies. However, the perforation is able to filter a range of the higher excitation frequencies, which are the ones that could potentially cause damage to the structure e.g. in the case of a hybrid joint.

5. Conclusions

The present study deals with frequency filtering phenomenon encountered in 2D lattice structures such as hybrid metal-composite joints. The study conducted is numerical and includes frequency eigenvalue extraction for a structure with holes. Since the study is generic the results may be applied to many disciplines, nonetheless, the emphasis here has been on the propagation of mechanical waves in 2D lattices of heterogeneous nature.

In this work a super-element has been formulated based on the finite element (FE) method by assembling four similar parts i.e. four quarters of a unit cell. As an example, one super-element with 50 dof has been adopted and studied. The degrees of freedom are reduced through static condensation. Subsequently, Floquet–Bloch's principle has been utilised to study wave filtering phenomenon in the representative building block (primitive cell) of the 2D lattice. In order to explore the shock response of a heterogeneous perforated 2D lattice, a frequency eigenvalue extraction analysis for the primitive cell has been conducted for the first Brillouin zone. The wave motion complex eigenvalue problem has been solved for given geometric input ratios, and the corresponding band structure diagrams are obtained.

The results show that frequency bands can be governed not only by the proportion of inclusion (resin filling) to the matrix (metallic part), but also by the structural geometric input ratios (i.e. by α and β). Existing literature shows that band gaps can be maximised by using higher contrast of inclusion to the matrix, however, a widened band may still not cover the frequency range which is desired to be filtered by the 2D lattice. Therefore, apart from using high contrast material in a heterogeneous perforated 2D lattice panel, one can optimise the perforated lattice panel to achieve desired band gap characteristics by varying the geometric input ratios α and β. Hence, elastic waves can be prevented from propagating or admitted to propagate in the specified frequency regimes by changing these parameters.

The results from the band structure diagrams in this study show that perforations may have limited effect on lower excitation frequencies, nevertheless, clearly complete forbidden bands are observed for a range of higher excitation frequencies. These higher frequencies are the ones which might cause dramatic and sudden failure to the hybrid joint in a high rate loading event such as a blast or impact scenario. This means, as expected, by applying perforations to the metal part of the hybrid joint, a beneficial filtering effect can be obtained if the response were to remain in the elastic range and linearity were to be preserved. The advantages of perforated lattice frequency filtering could be utilised to protect the joints subjected to impulsive or pulse loads, thus, to improve their shock response behaviour. However when nonlinearities are involved this would be an extremely intricate problem which merits to be addressed in a separate study.

Acknowledgements

The authors should like to express their thanks to Dr. A. Mostofi of the Department of Material Sciences at Imperial College London for fruitful discussions during the preparation of the manuscript. Also to Mr. R. Ward of the Department of Physics at Imperial College London who provided invaluable insight into *k*-space formulation of the lattice problem.

Appendix A. Derived shape function matrix for a 3×3 Lagrangian element

$$\mathbf{HI^T} = \begin{bmatrix} 1/4*r*(r-1)*s*(s-1) & 0 \\ 0 & 1/4*r*(r-1)*s*(s-1) \\ -1/2*(r+1)*(r-1)*s*(s-1) & 0 \\ 0 & -1/2*(r+1)*(r-1)*s*(s-1) \\ 1/2*(1/2*r+1/2)*r*s*(s-1) & 0 \\ 0 & 1/2*(1/2*r+1/2)*r*s*(s-1) \\ -1/2*r*(r-1)*(s+1)*(s-1) & 0 \\ 0 & -1/2*r*(r-1)*(s+1)*(s-1) \\ (r+1)*(r-1)*(s+1)*(s-1) & 0 \\ 0 & (r+1)*(r-1)*(s+1)*(s-1) \\ -(1/2*r+1/2)*r*(s+1)*(s-1) & 0 \\ 0 & -(1/2*r+1/2)*r*(s+1)*(s-1) \\ 1/2*r*(r-1)*(1/2*s+1/2)*s & 0 \\ 0 & 1/2*r*(r-1)*(1/2*s+1/2)*s \\ -(r+1)*(r-1)*(1/2*s+1/2)*s & 0 \\ 0 & -(r+1)*(r-1)*(1/2*s+1/2)*s \\ (1/2*r+1/2)*r*(1/2*s+1/2)*s & 0 \\ 0 & (1/2*r+1/2)*r*(1/2*s+1/2)*s \end{bmatrix}$$

Appendix B. Derived Jacobian matrix for a 3×3 Lagrangian element

$$\begin{aligned} \mathbf{JI} = [&-1/2*(r-1)*(1/2*s+1/2)*s*a - 1/2*(r+1)*(1/2*s+1/2)*s*a + 1/2*(r-1)*(s+1)*(s-1)*a \\ &+ 1/2*(r+1)*(s+1)*(s-1)*a - 1/4*(r-1)*s*(s-1)*a - 1/4*(r+1)*s*(s-1)*a \\ &+ 1/2*r*(1/2*s+1/2)*s*a + (1/2*r+1/2)*(1/2*s+1/2)*s*a - 1/2*r*(s+1)*(s-1)*a \\ &- (1/2*r+1/2)*(s+1)*(s-1)*a + 1/4*r*s*(s-1)*a + 1/2*(1/2*r+1/2)*s*(s-1)*a, \\ &- 1/2*(r-1)*(1/2*s+1/2)*s*c + r*(1/2*s+1/2)*s*c + 1/4*(r-1)*(s+1)*(s-1)*c \\ &- 1/2*r*(s+1)*(s-1)*c - (r+1)*(1/2*s+1/2)*s*c + 1/2*(r+1)*(s+1)*(s-1)*c \\ &+ (1/2*r+1/2)*(1/2*s+1/2)*s*c - 1/2*(1/2*r+1/2)*(s+1)*(s-1)*c] \\ [&-1/2*(r+1)*(r-1)*s*a - 1/2*(r+1)*(r-1)*(1/2*s+1/2)*a + 1/4*(r+1)*(r-1)*(s-1)*a \\ &+ 1/2*(r+1)*(r-1)*(s+1)*a + (1/2*r+1/2)*r*s*a + (1/2*r+1/2)*r*(1/2*s+1/2)*a \\ &- 1/2*(1/2*r+1/2)*r*(s-1)*a - (1/2*r+1/2)*r*(s+1)*a, 1/4*r*(r-1)*s*c \\ &+ 1/2*r*(r-1)*(1/2*s+1/2)*c - 1/4*r*(r-1)*(s-1)*c - 1/4*r*(r-1)*(s+1)*c \\ &- 1/2*(r+1)*(r-1)*s*c - (r+1)*(r-1)*(1/2*s+1/2)*c + 1/2*(r+1)*(r-1)*(s-1)*c \\ &+ 1/2*(r+1)*(r-1)*(s+1)*c + 1/2*(1/2*r+1/2)*r*s*c + (1/2*r+1/2)*r*(1/2*s+1/2)*c \\ &- 1/2*(1/2*r+1/2)*r*(s-1)*c - 1/2*(1/2*r+1/2)*r*(s+1)*c] \end{aligned}$$

Appendix C. Matlab 7.5 scripts

Matlab 7.5 script 1

```
function [sf] = Phix(j,X,N,r)
sf = 1;
for n = 1:N
  if (n~ = j)
    sf = sf*(r-X(n))/(X(j)-X(n));end
end
End
```

Matlab 7.5 script 2

```
for i = 1:P
  for j = 1:N
HIa(i,j) = Phix(j,X,N,r)*Phiy(i,PY,P,s);
  end
End
HIa
```

Matlab 7.5 script 3

```
[risi_N,weight_N] = GS(GSN,GSra,GSrb);
[risi_P,weight_P] = GS(GSP,GSra,GSrb);
  Fmass_a = HIT*HI*dJI;
*******************************
Fmass_b = zeros(P*N*2,P*N*2);
for risi_Ni = 1:GSN
  for risi_Pi = 1:GSP
    r = risi_N(risi_Ni,1);
    s = risi_P(risi_Pi,1);
Fmass_b = Fmass_b+weight_N(risi_Ni,1)
*weight_P(risi_Pi,1).*subs(Fmass_a);
syms r s
  end
end
MassI = simplify(rus*t*Fmass_b);
```

Matlab 7.5 script 4

```
function [risi,weight] = GS(GSn,GSra,GSrb)
GSn = GSn-1;
GSn1 = GSn+1; GSn2 = GSn+2;
xu = linspace(-1,1,GSn1)';
% Initial guess
y = cos((2*(0:GSn)'+1)*pi/(2*GSn+2))+(0.27/GSn1)*sin(pi*xu*GSn/GSn2);
% Legendre-Gauss Vandermonde Matrix
L = zeros(GSn1,GSn2);
% Derivative of LGVM
Lp = zeros(GSn1,GSn2);
% Compute the zeros of the GSn+1 Legendre Polynomial
% using the recursion relation and the Newton-Raphson method
y0 = 2;
% Iterate until new points are uniformly within epsilon of old points
while max(abs(y-y0))>eps
  L(:,1) = 1;
  Lp(:,1) = 0;
  L(:,2) = y;
  Lp(:,2) = 1;
  for k = 2:GSn1
    L(:,k+1) = ( (2*k-1)*y.*L(:,k)-(k-1)*L(:,k-1) )/k; end
  Lp = (GSn2).*( L(:,GSn1)-y.*L(:,GSn2) )./(1-y.^2);
  y0 = y;
  y = y0-L(:,GSn2)./Lp; end
risi = (GSra*(1-y)+GSrb*(1+y))/2; % Linear map from[-1,1] to [GSra,GSrb]
weight = (GSrb-GSra)./((1-y.^2).*Lp.^2)*(GSn2/GSn1)^2; %Compute weights
```

Appendix D

Derived mass matrix for a 3×3 Lagrangian element:

$$\mathbf{MI}_{3\times 3} = 1.0\mathrm{e}^{-7} \begin{bmatrix}
1.43 & 0 & 0.72 & 0 & -0.36 & 0 & 0.72 & 0 & 0.36 & 0 & -0.18 & 0 & -0.36 & 0 & -0.18 & 0 & 0.09 & 0 \\
\ldots & 1.43 & 0 & 0.72 & 0 & -0.36 & 0 & 0.72 & 0 & 0.36 & 0 & -0.18 & 0 & -0.36 & 0 & -0.18 & 0 & 0.09 \\
\ldots & \ldots & 5.73 & 0 & 0.72 & 0 & 0.36 & 0 & 2.87 & 0 & 0.36 & 0 & -0.18 & 0 & -1.43 & 0 & -0.18 & 0 \\
\ldots & \ldots & \ldots & 5.73 & 0 & 0.72 & 0 & 0.36 & 0 & 2.87 & 0 & 0.36 & 0 & -0.18 & 0 & -1.43 & 0 & -0.18 \\
\ldots & \ldots & \ldots & \ldots & 1.43 & 0 & -1.18 & 0 & 0.36 & 0 & 0.72 & 0 & 0.09 & 0 & -0.18 & 0 & -0.36 & 0 \\
\ldots & \ldots & \ldots & \ldots & \ldots & 1.43 & 0 & -0.18 & 0 & 0.36 & 0 & 0.72 & 0 & 0.09 & 0 & -0.18 & 0 & -0.36 \\
\ldots & \ldots & \ldots & \ldots & \ldots & \ldots & 5.73 & 0 & 287 & 0 & -1.43 & 0 & 0.72 & 0 & 0.36 & 0 & -0.18 & 0 \\
\ldots & \ldots & \ldots & \ldots & \ldots & \ldots & \ldots & 5.73 & 0 & 287 & 0 & -1.43 & 0 & 0.72 & 0 & 0.36 & 0 & -0.18 \\
\ldots & \ldots & \ldots & \ldots & \ldots & \ldots & \ldots & \ldots & 22.93 & 0 & 2.87 & 0 & 0.36 & 0 & 2.87 & 0 & 0.36 & 0 \\
\text{Symmetric} & & & & & & & & & & & & & & & & & \\
\ldots & \ldots & \ldots & \ldots & \ldots & \ldots & \ldots & \ldots & \ldots & 22.93 & 0 & 2.87 & 0 & 0.36 & 0 & 2.87 & 0 & 0.36 \\
\ldots & \ldots & \ldots & \ldots & \ldots & \ldots & \ldots & \ldots & \ldots & \ldots & 5.73 & 0 & -0.18 & 0 & 0.36 & 0 & 0.72 & 0 \\
\ldots & \ldots & \ldots & \ldots & \ldots & \ldots & \ldots & \ldots & \ldots & \ldots & \ldots & 5.73 & 0 & -0.18 & 0 & 0.36 & 0 & 0.72 \\
\ldots & \ldots & \ldots & \ldots & \ldots & \ldots & \ldots & \ldots & \ldots & \ldots & \ldots & \ldots & 1.43 & 0 & 0.72 & 0 & -0.36 & 0 \\
\ldots & \ldots & \ldots & \ldots & \ldots & \ldots & \ldots & \ldots & \ldots & \ldots & \ldots & \ldots & \ldots & 1.43 & 0 & 0.72 & 0 & -0.36 \\
\ldots & \ldots & \ldots & \ldots & \ldots & \ldots & \ldots & \ldots & \ldots & \ldots & \ldots & \ldots & \ldots & \ldots & 5.73 & 0 & 0.72 & 0 \\
\ldots & \ldots & \ldots & \ldots & \ldots & \ldots & \ldots & \ldots & \ldots & \ldots & \ldots & \ldots & \ldots & \ldots & \ldots & 5.73 & 0 & 0.72 \\
\ldots & \ldots & \ldots & \ldots & \ldots & \ldots & \ldots & \ldots & \ldots & \ldots & \ldots & \ldots & \ldots & \ldots & \ldots & \ldots & 1.43 & 0 \\
\ldots & \ldots & \ldots & \ldots & \ldots & \ldots & \ldots & \ldots & \ldots & \ldots & \ldots & \ldots & \ldots & \ldots & \ldots & \ldots & \ldots & 1.43
\end{bmatrix} \cdot \mathbf{ac}$$

Derived Stiffness Matrix for a 3×3 Lagrangian Element:

$$\mathbf{k_e I_{3\times 3}} = \begin{bmatrix}
k_{1,1} & k_{1,2} & k_{1,3} & k_{1,4} & k_{1,5} & k_{1,6} & k_{1,7} & k_{1,8} & k_{1,9} & k_{1,10} & k_{1,11} & k_{1,12} & k_{1,13} & k_{1,14} & k_{1,15} & k_{1,16} & k_{1,17} & k_{1,18} \\
\cdots & k_{2,2} & k_{2,3} & k_{2,4} & k_{2,5} & k_{2,6} & k_{2,7} & k_{2,8} & k_{2,9} & k_{2,10} & k_{2,11} & k_{2,12} & k_{2,13} & k_{2,14} & k_{2,15} & k_{2,16} & k_{2,17} & k_{2,18} \\
\cdots & \cdots & k_{3,3} & 0 & k_{3,5} & k_{3,6} & k_{3,7} & k_{3,8} & k_{3,9} & 0 & k_{3,11} & k_{3,12} & k_{3,13} & k_{3,14} & k_{3,15} & 0 & k_{3,17} & k_{3,18} \\
\cdots & \cdots & \cdots & k_{4,4} & k_{4,5} & k_{4,6} & k_{4,7} & k_{4,8} & 0 & k_{4,10} & k_{4,11} & k_{4,12} & k_{4,13} & k_{4,14} & 0 & k_{4,16} & k_{4,17} & k_{4,18} \\
\cdots & \cdots & \cdots & \cdots & k_{5,5} & k_{5,6} & k_{5,7} & k_{5,8} & k_{5,9} & k_{5,10} & k_{5,11} & k_{5,12} & k_{5,13} & k_{5,14} & k_{5,15} & k_{5,16} & k_{5,17} & k_{5,18} \\
\cdots & \cdots & \cdots & \cdots & \cdots & k_{6,6} & k_{6,7} & k_{6,8} & k_{6,9} & k_{6,10} & k_{6,11} & k_{6,12} & k_{6,13} & k_{6,14} & k_{6,15} & k_{6,16} & k_{6,17} & k_{6,18} \\
\cdots & \cdots & \cdots & \cdots & \cdots & \cdots & k_{7,7} & 0 & k_{7,9} & 0 & k_{7,11} & 0 & k_{7,13} & k_{7,14} & k_{7,15} & k_{7,16} & k_{7,17} & k_{7,18} \\
\cdots & \cdots & \cdots & \cdots & \cdots & \cdots & \cdots & k_{8,8} & 0 & k_{8,10} & 0 & k_{8,12} & k_{8,13} & k_{8,14} & k_{8,15} & k_{8,16} & k_{8,17} & k_{8,18} \\
\cdots & \cdots & \cdots & \cdots & \cdots & \cdots & \cdots & \cdots & k_{9,9} & 0 & k_{9,11} & 0 & k_{9,13} & k_{9,14} & k_{9,15} & 0 & k_{9,17} & k_{9,18} \\
\cdots & \cdots & \cdots & \cdots & \cdots & \cdots & \cdots & \cdots & \cdots & k_{10,10} & 0 & k_{10,12} & k_{10,13} & k_{10,14} & 0 & k_{10,16} & k_{10,17} & k_{10,18} \\
\text{Symmetric} & & & & & & & & & & & & & & & & & \\
\cdots & \cdots & \cdots & \cdots & \cdots & \cdots & \cdots & \cdots & \cdots & \cdots & k_{11,11} & 0 & k_{11,13} & k_{11,14} & k_{11,15} & k_{11,16} & k_{11,17} & k_{11,18} \\
\cdots & \cdots & \cdots & \cdots & \cdots & \cdots & \cdots & \cdots & \cdots & \cdots & \cdots & k_{12,12} & k_{12,13} & k_{12,14} & k_{12,15} & k_{12,16} & k_{12,17} & k_{12,18} \\
\cdots & \cdots & \cdots & \cdots & \cdots & \cdots & \cdots & \cdots & \cdots & \cdots & \cdots & \cdots & k_{13,13} & k_{13,14} & k_{13,15} & k_{13,16} & k_{13,17} & k_{13,18} \\
\cdots & \cdots & \cdots & \cdots & \cdots & \cdots & \cdots & \cdots & \cdots & \cdots & \cdots & \cdots & \cdots & k_{14,14} & k_{14,15} & k_{14,16} & k_{14,17} & k_{14,18} \\
\cdots & \cdots & \cdots & \cdots & \cdots & \cdots & \cdots & \cdots & \cdots & \cdots & \cdots & \cdots & \cdots & \cdots & k_{15,15} & 0 & k_{15,17} & k_{15,18} \\
\cdots & \cdots & \cdots & \cdots & \cdots & \cdots & \cdots & \cdots & \cdots & \cdots & \cdots & \cdots & \cdots & \cdots & \cdots & k_{16,16} & k_{16,17} & k_{16,18} \\
\cdots & \cdots & \cdots & \cdots & \cdots & \cdots & \cdots & \cdots & \cdots & \cdots & \cdots & \cdots & \cdots & \cdots & \cdots & \cdots & k_{17,17} & k_{17,18} \\
\cdots & \cdots & \cdots & \cdots & \cdots & \cdots & \cdots & \cdots & \cdots & \cdots & \cdots & \cdots & \cdots & \cdots & \cdots & \cdots & \cdots & k_{18,18}
\end{bmatrix}$$

$$\mathbf{k_{1,6}} = \mathbf{k_{2,13}} = \mathbf{k_{5,18}} = \mathbf{k_{14,17}} = 0.89; \quad \mathbf{k_{1,14}} = \mathbf{k_{2,5}} = \mathbf{k_{6,17}} = \mathbf{k_{13,18}} = -0.89;$$

$$\mathbf{k_{1,2}} = \mathbf{k_{17,18}} = 34.82; \quad \mathbf{k_{5,6}} = \mathbf{k_{13,14}} = -34.82;$$

$$\mathbf{k_{1,8}} = \mathbf{k_{2,3}} = \mathbf{k_{4,5}} = \mathbf{k_{6,11}} = \mathbf{k_{7,14}} = \mathbf{k_{12,17}} = \mathbf{k_{13,16}} = \mathbf{k_{15,18}} = 3.57;$$
$$\mathbf{k_{1,4}} = \mathbf{k_{2,7}} = \mathbf{k_{3,6}} = \mathbf{k_{5,12}} = \mathbf{k_{8,13}} = \mathbf{k_{11,18}} = \mathbf{k_{14,15}} = \mathbf{k_{16,17}} = -3.57;$$

$$\mathbf{k_{1,12}} = \mathbf{k_{1,16}} = \mathbf{k_{2,11}} = \mathbf{k_{2,15}} = \mathbf{k_{3,18}} = \mathbf{k_{4,17}} = \mathbf{k_{7,18}} = \mathbf{k_{8,17}} = 15.5;$$
$$\mathbf{k_{3,14}} = \mathbf{k_{4,13}} = \mathbf{k_{5,8}} = \mathbf{k_{5,16}} = \mathbf{k_{6,7}} = \mathbf{k_{6,15}} = \mathbf{k_{11,14}} = \mathbf{k_{12,13}} = -15.5;$$

$$\mathbf{k_{3,8}} = \mathbf{k_{4,7}} = \mathbf{k_{5,10}} = \mathbf{k_{6,9}} = \mathbf{k_{9,14}} = \mathbf{k_{10,13}} = \mathbf{k_{11,16}} = \mathbf{k_{12,15}} = 61.9;$$
$$\mathbf{k_{1,10}} = \mathbf{k_{2,9}} = \mathbf{k_{3,12}} = \mathbf{k_{4,11}} = \mathbf{k_{7,16}} = \mathbf{k_{8,15}} = \mathbf{k_{9,18}} = \mathbf{k_{10,17}} = -61.9;$$

$$\mathbf{k_{1,18}} = \mathbf{k_{2,17}} = -3.87; \quad \mathbf{k_{5,14}} = \mathbf{k_{6,13}} = 3.87;$$

$$\mathbf{k_{1,5}} = \mathbf{k_{13,17}} = 9.25 \cdot \zeta - 5.83/\zeta; \quad \mathbf{k_{2,14}} = \mathbf{k_{6,18}} = -5.83 \cdot \zeta + 9.52/\zeta;$$

$$\mathbf{k_{1,1}} = \mathbf{k_{5,5}} = \mathbf{k_{13,13}} = \mathbf{k_{17,17}} = 66.67 \cdot \zeta + 23.33/\zeta; \quad \mathbf{k_{2,2}} = \mathbf{k_{6,6}} = \mathbf{k_{14,14}} = \mathbf{k_{18,18}} = 23.33 \cdot \zeta + 66.67/\zeta;$$

$$\mathbf{k_{1,3}} = \mathbf{k_{3,5}} = \mathbf{k_{13,15}} = \mathbf{k_{15,17}} = -76.19 \cdot \zeta + 11.67/\zeta; \quad \mathbf{k_{2,8}} = \mathbf{k_{6,12}} = \mathbf{k_{8,14}} = \mathbf{k_{12,18}} = 11.67 \cdot \zeta - 76.19/\zeta;$$

$$\mathbf{k_{1,7}} = \mathbf{k_{5,11}} = \mathbf{k_{7,13}} = \mathbf{k_{11,17}} = 33.33 \cdot \zeta - 26.67/\zeta; \quad \mathbf{k_{2,4}} = \mathbf{k_{4,6}} = \mathbf{k_{14,16}} = \mathbf{k_{16,18}} = -26.67 \cdot \zeta + 33.33/\zeta;$$

$$\mathbf{k_{1,9}} = \mathbf{k_{3,7}} = \mathbf{k_{3,11}} = \mathbf{k_{5,9}} = \mathbf{k_{7,15}} = \mathbf{k_{9,13}} = \mathbf{k_{9,17}} = \mathbf{k_{11,15}} = -38.1 \cdot \zeta - 13.3/\zeta;$$
$$\mathbf{k_{3,15}} = -38.1 \cdot \mathrm{A} + 13.33/\zeta; \quad \mathbf{k_{7,11}} = 38.1 \cdot \zeta - 13.33/\zeta;$$

$$\mathbf{k_{2,10}} = \mathbf{k_{4,8}} = \mathbf{k_{4,12}} = \mathbf{k_{6,10}} = \mathbf{k_{8,16}} = \mathbf{k_{10,14}} = \mathbf{k_{10,18}} = \mathbf{k_{12,16}} = -13.33 \cdot \zeta - 38.1/\zeta;$$
$$\mathbf{k_{8,12}} = 13.3 \cdot \mathrm{A} - 38.1/\zeta; \quad \mathbf{k_{4,16}} = -13.3 \cdot \zeta + 38.1/\zeta;$$

$$\mathbf{k_{1,11}} = \mathbf{k_{2,16}} = \mathbf{k_{5,7}} = \mathbf{k_{7,17}} = \mathbf{k_{11,13}} = 4.76 \cdot \zeta + 6.67/\zeta;$$
$$\mathbf{k_{2,16}} = \mathbf{k_{4,14}} = \mathbf{k_{4,18}} = \mathbf{k_{6,16}} = 6.67 \cdot \zeta + 4.76/\zeta;$$

$$\mathbf{k_{1,13}} = \mathbf{k_{5,17}} = -16.67 \cdot \zeta + 3.33/\zeta; \quad \mathbf{k_{2,6}} = \mathbf{k_{14,18}} = 3.33 \cdot \zeta - 16.67/\zeta;$$

$$\mathbf{k_{1,15}} = \mathbf{k_{3,13}} = \mathbf{k_{3,17}} = \mathbf{k_{5,15}} = 19.05 \cdot \zeta + 1.67/\zeta; \quad \mathbf{k_{2,12}} = \mathbf{k_{6,8}} = \mathbf{k_{8,18}} = \mathbf{k_{12,14}} = 1.67 \cdot \zeta + 19.05/\zeta;$$

$$\mathbf{k_{1,17}} = \mathbf{k_{5,13}} = -2.38 \cdot \zeta - 0.83/\zeta; \quad \mathbf{k_{2,18}} = \mathbf{k_{6,14}} = -0.83 \cdot \zeta - 2.38/\zeta;$$

$$\mathbf{k}_{3,3} = \mathbf{k}_{15,15} = 152.38 \cdot \zeta + 93.33/\zeta; \quad \mathbf{k}_{8,8} = \mathbf{k}_{12,12} = 93.33 \cdot \zeta + 152.38/\zeta;$$

$$\mathbf{k}_{4,4} = \mathbf{k}_{16,16} = 53.33 \cdot \zeta + 266.67/\zeta; \quad \mathbf{k}_{7,7} = \mathbf{k}_{11,11} = 266.67 \cdot \zeta + 53.33/\zeta;$$

$$\mathbf{k}_{3,9} = \mathbf{k}_{9,15} = 76.19 \cdot \zeta - 106.67/\zeta; \quad \mathbf{k}_{8,10} = \mathbf{k}_{10,12} = -106.67 \cdot \zeta + 76.19/\zeta;$$

$$\mathbf{k}_{4,10} = \mathbf{k}_{10,16} = 26.67 \cdot \zeta - 304.76/\zeta; \quad \mathbf{k}_{7,9} = \mathbf{k}_{9,11} = -304.76 \cdot \zeta + 26.67/\zeta;$$

$$\mathbf{k}_{9,9} = 609.52 \cdot \zeta + 213.33/\zeta; \quad \mathbf{k}_{10,10} = 213.33 \cdot \zeta + 609.52/\zeta;$$

where $\zeta = c/a$.

References

[1] M.A. Bravais, *On the systems formed by points regularly distributed on a plane or in space*, Dover Publications, New York, 1949.
[2] D.J. Mead, Wave propagation in continuous periodic structures: research contributions from Southampton, 1964–1995, *Journal of Sound and Vibration* 190 (3) (1996) 495–524.
[3] L.J. Gibson, M.F. Ashby, *Cellular Solids: Structure and Properties*, 2nd ed., Cambridge University Press, Cambridge, 1997.
[4] L. Brillouin, *Wave Propagation Periodic Structures—Electric Filters and Crystal Lattices*, 2nd ed., Dover Publications, New York, 1953.
[5] L. Rayleigh, On the maintenance of vibrations by forces of double frequency, and on the propagation of waves through a medium endowed with a periodic structure, *Philosophical Magazine* 24 (1887) 145–159.
[6] W.F.P. Knipping, M. Laue, Interference effects with Rontgen rays, *Sitzungsberichte der Bayerischen Akademie de Wissenschaften, math.-phy. Klasse*, 1912, pp. 303–322.
[7] C. Kittel, *Elementary Solid State Physics: A Short Course*, 1st ed., Wiley, New York, 1962.
[8] F. Bloch, Uber die Quantenmechanik der Electron in Kristallgittern (On the quantum mechanics of the Electron in crystal lattices), *Zeifschrift fur Physik* 52 (1928) 555–600.
[9] C. Kittel, *Introduction to Solid State Physics*, 4th ed., Wiley, New York, 1971.
[10] Z. Zhang, S. Satpathy, Electromagnetic wave propagation in periodic structures: Bloch wave solution of Maxwell's equation, *Physical Review Letters* 65 (1990) 2650–2653.
[11] E. Yablonovitch, E.O. Kane, Band structure engineering of semiconductor lasers for optical communications, *Journal of Lightwave Technology* 6 (8) (1988) 1292–1299.
[12] M. Rim, Y. Kim, Narrowband noise attenuation characteristics of in-duct acoustic screens, *Journal of Sound and Vibration* 234 (5) (2000) 737–759.
[13] J.W. Fleischer, M. Segev, N.K. Efremidis, D.N. Christodoulides, Observation of two-dimensional discrete solitons in optically-induced nonlinear photonic lattices, *Nature* 422 (2003) 147–150.
[14] E. Yablonovitch, T.J. Gmitter, K.M. Leung, Photonic band structure: the face-centered-cubic case employing nonspherical atoms, *Physical Review Letters* 67 (17) (1991) 2295–2299.
[15] A.R. Diaz, A.G. Haddow, L. Ma, Design of band-gap grid structures, *Structural and Multidisciplinary Optimization* (2005) 418–431.
[16] J.S. Jensen, Phononic band gaps and vibrations in one- and two-dimensional mass–spring structures, *Journal of Sound and Vibration* 266 (2003) 1053–1078.
[17] P.W. Anderson, N. Mott, Nobel Lectures in Physics for 1977, *Reviews of Modern Physics* (1978) 191–208.
[18] Y. Rahmat-Samii, H. Mosallaei, Electromagnetic band-gap structures: classification, characterization, and applications, *Eleventh International Conference on Antennas and Propagation*, IEE Conference, Publ. No. 480, Vol. 2, 2001, pp. 560–564.
[19] C.A. Gentry, C. Guigou, C.R. Fuller, Smart foam for applications in passive–active noise radiation control, *Journal of Sound and Vibration* 266 (2003) 1711–1718.
[20] H.K. Pelton, S. Wise, W.S. Sims, Active HVAC noise control systems provide acoustical comfort, *Journal of Sound and Vibration* (1994) 14–18.
[21] Y. Lai, X.D. Zhang, Z.Q. Zhang, Engineering acoustic band gaps, *Applied Physics Letters* 79 (20) (2001) 3224–3226.
[22] M.M. Sigalas, E.N. Economou, Elastic and acoustic wave band structure, *Journal of Sound and Vibration* 158 (2) (1992) 377–382.
[23] D.J. Mead, A general theory of harmonic wave propagation in linear periodic systems with multiple coupling, *Journal of Sound and Vibration* 27 (1973) 235–260.
[24] M.A. Hawwa, Reflection of flexural waves in geometrically periodic beams, *Journal of Sound and Vibration* (1997) 453–461.
[25] G. Evans, J.W. Hutchinson, N.A. Fleck, M.F. Ashby, H.N.G. Wadley, The topological design of multifunctional cellular metals, *Progress in Materials Science* 46 (3–4) (2001) 309–327.
[26] G.S. Gupta, Natural flexural waves and the normal modes of periodically-supported beams and plates, *Journal of Sound and Vibration* 13 (1970) 89–101.
[27] N. Wicks, J.W. Hutchinson, Optimal truss plates, *International Journal of Solids and Structures* 38 (2001) 5165–5183.
[28] H. Unden, S. Ridder, Loading-introducing armature as component part of a laminated structural element, United States Patent No. 4673606, 1987.
[29] J.D. Melograna, J.L. Grenestedt, Improving joints between composites and steel using perforations, *Composites: Part A* 33 (2002) 1253–1261.
[30] J. Cao, J.L. Grenestedt, Design and testing of joints for composite sandwich/steel hybrid ship hulls, *Composites: Part A* 35 (2004) 1091–1105.
[31] K.J. Bathe, *Finite Element Procedures*, Prentice Hall, New York, 1982.
[32] R.R. Craig, A.J. Kurdila, *Fundamental of Structural Dynamics*, 2nd ed., Wiley, New York, 2006.
[33] O. Sigmund, J.S. Jensen, Topology optimization of phononic band gap materials and structures, *Fifth World Congress on Computational Mechanics*, Vienna, Austria, 2002.
[34] A.S. Phani, J. Woodhouse, N.A. Fleck, Wave propagation in two-dimensional periodic lattices, *Journal of Acoustical Society of America* 119 (4) (2006) 1995–2005.
[35] H. Ibach, H. Luth, *Solid State Physics*, Springer, Berlin, 2003.